CHAPTER 3

Tau-p PROCESSING IN SYNTHETIC SEISMIC DATA

The application of *tau-p* processing is to improve the quality of deep seismic data by using linear and parabolic *tau-p* processing, and then compare the efficiency of the *tau-p* processing with the conventional processing.

3.1 *Tau-p* processing

3.1.1 Linear tau-p processing

The linear *tau-p* processing in this study is produced by Dunne and Beresford (1998). It was used for improving deep seismic data by, *firstly*, rearrange data for processing in the common mid point (CMP) domain. In the CMP domain, p represents the average horizontal slowness of the up-going and down-going waves; for moderate dips. This helps to maintain purity in the plane-wave decomposition (Diebold and Stoffa, 1981). *Secondly*, applying supergather to attenuate the ground rolls energy and improve the quality of signal. The supergather was processed on summing nearby CMP over offset such as the center CMP, i.e. 250 and Bin of CMP, i.e. 3. It is a mean summation on the offset of CMP, i.e. 247,248,249,250,251,252 and 253, for example. The characters of reflectors (intercept time, moveout and velocity) have not change however only the numbers of traces are increased. *Thirdly*, linear *tau-p* transformation was applied following hyperbolic velocity filter (HVF) designed from equation (2.35) to suppress the transform artifacts. *Finally*, applying gap deconvolution to suppress multiples in linear *tau-p* domain because of the multiples are periodicity in along the p direction (Taner, 1980). Although this study does not have well log data, to design the gap deconvolution parameters, the predictive deconvolution will be used instead.

3.1.2 Parabolic tau-p processing

The parabolic *tau-p* processing in this study is applied from Spitzer *et al.* (2003). This processing technique flattens primary events with NMO correction, leaving multiples approximately parabolic on the CMP gathers. The parabolic *tau-p* transform is applied following scaling (sign square) to enhance relative signal to random noise energy because the parabolic *tau-p* transform increase the reflected signal to noise ratio (S/N) ~ 10, therefore remnants have lower amplitudes then the reflections. By simply scaling the value of each sample in the parabolic *tau-p* domain, the S/N is increase further ~100 (employing the higher power to data results in greater amplitude distortions). The characters of reflectors and multiples are separated in parabolic *tau-p* domain which presented at $q = 0$ and $q > 0$, respectively, then the multiples can be suppressed. The true amplitude is distorted during parabolic *tau-p* transformation then the re-scaling (sign square root) is applied to preserve the relative amplitude variations along the individual traces. After inverse parabolic *tau-p* transformation, the energy of multiples is remnant (the curvature of multiples is nearly with the reflectors) then the predictive deconvolution is assigned to correct this problem.

The steps processing of each method is shown in Figure 3.1.

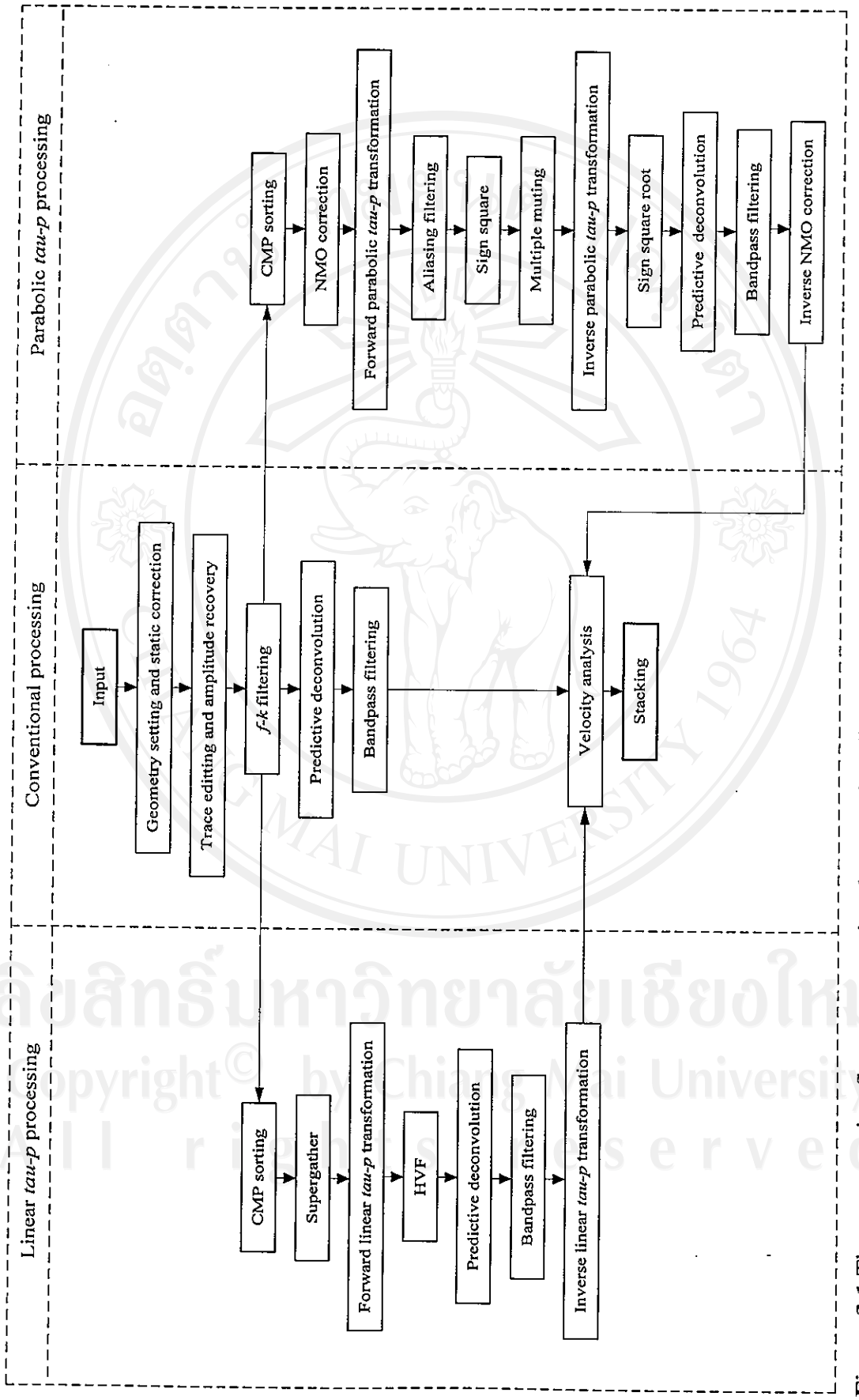

Figure 3.1 Three processing flows, conventional processing, linear *tau-p* processing and parabolic *tau-p* processing.

3.2 Linear *tau-p* processing in synthetic seismic data

The 11 processing steps (Figure 3.1 some processes are not necessary) and the parameters in the linear *tau-p* processing are presented in Table 3.1.

Table 3.1 Processing steps and parameters of synthetic data in the linear *tau-p* processing.

Processing	Remark
1. Geometry setting and static correction	
2. Trace editing and amplitude recovery	mute refracted wave and exponential gain = 0.5
3. CMP sorting	rearrange data (shot ⟶ CMP)
4. Supergather	3 CMPs to 1 Supergather
5. Forward linear *tau-p* processing	sample interval = 25 m, max, min *tau-p* slope = $\pm 750\times10^{-6}$ s/m, No. of slope = No. of trace input
6. HVF	k = 15%, velocity function *B.SynVel1*
7. Predictive deconvolution	n = 300 ms, α = 88 ms, ε = 0.1%
8. Filtering	2/7-35/40 Hz
9. Inverse linear *tau-p* processing	restore the input record
10. Velocity analysis	output : velocity function *B.SynVel2*
11. Stacking	output : stack section

The sequence for linear *tau-p* processing in Table 3.1 is described as follows:

Step 1 and *Step 2* are similar to the conventional processing in synthetic data.

Step 3: To rearrange data from the common shot domain to the common mid point (CMP) domain.

Step 4: To improve the quality of seismic data. The number of seismic traces in CMP domain is increased from 30 trace to 90 trace (Figure 1.2 (b) and 3.2 (b)).

Step 5: To transform data in *t-x* domain to linear *tau-p* domain where the parameters of the maximum and the minimum *tau-p* slope are obtained from the minimum velocity of the velocity analysis where is 1360 m/s, thus will obtain the maximum slowness (*1/v*) is 1/1360 ≈ 750 μs/m. Figure 3.3 (a) shows forward linear

tau-p transform, the reflectors are transformed from hyperbolic events in *t-x* domain into elliptic events in linear *tau-p* domain.

Step 6: To reduce aliasing problem during the transformation. The HVF is designed from Equation (2.35) by applied velocity function *B.SynVel1* from the conventional processing (Figure 3.3 (b)).

Step 7: To eliminate multiples in the linear *tau-p* domain where all parameters are designed from auto-correlation and tested by a trial-error method.

Step 8: After applying predictive deconvolution, the bandpass filter is applied (Figure 3.4 (a)).

Step 9: To transform data in linear *tau-p* domain to *t-x* domain by using the same forward transformation parameters (Figure 3.4 (b)). After linear *tau-p* processing, the seismic signal is improved, it is often necessary to examine the new velocity analysis.

Step 10: Semblance analysis, common offset stack and common velocity stack compose the velocity analysis to obtain the velocity function (*B.SynVel2* ; Figure 3.5).

Step 11: NMO correction by using velocity function *B.SynlVel2* and stacking to obtain the stack section (Figure 3.6).

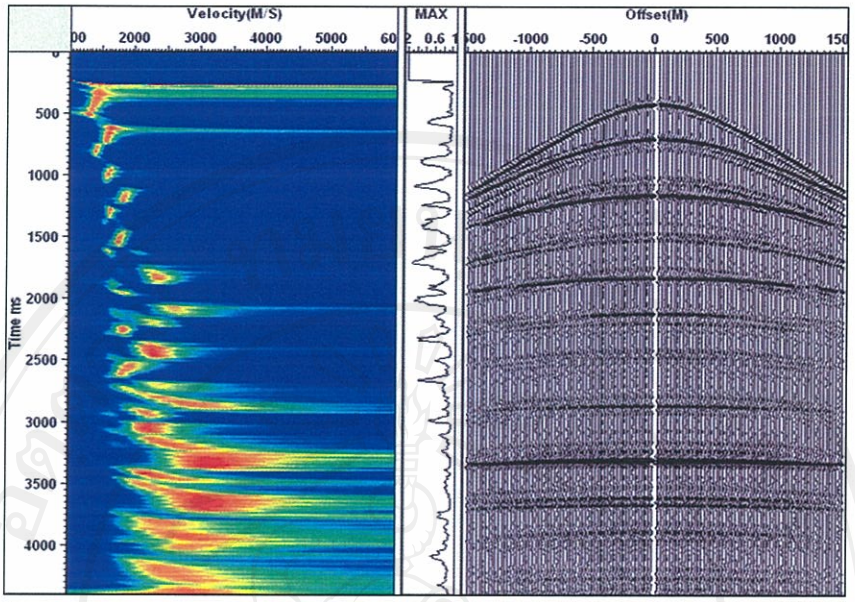

(a) (b)

Figure 3.2 (a) Velocity energy spectrum of CMP after supergather. (b) CMP after supergather that 3 CMPs to 1 Supergather (90 traces).

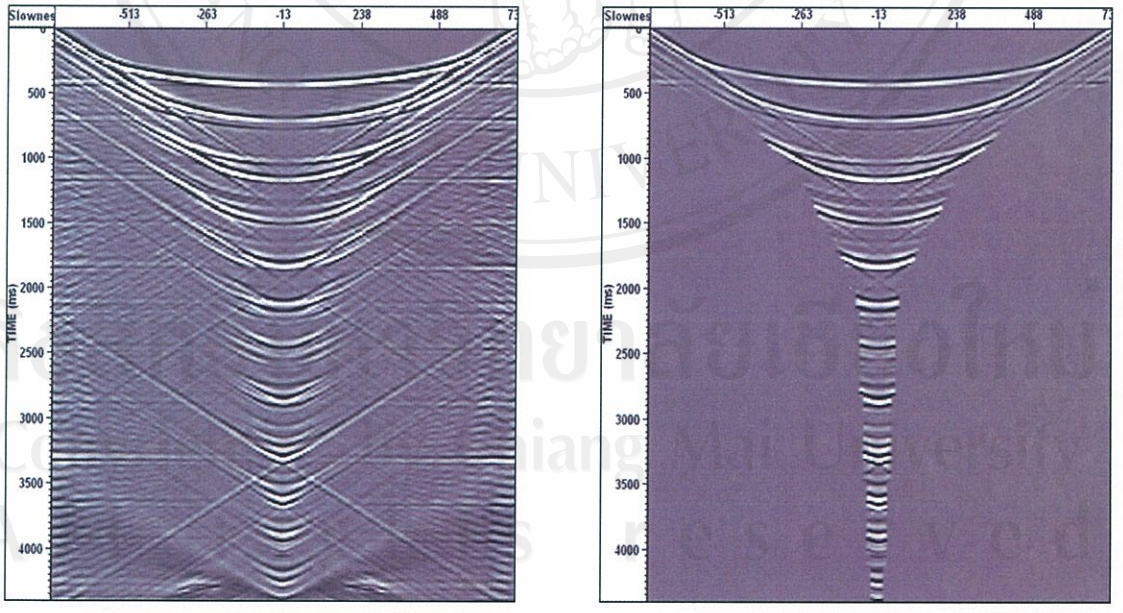

(a) (b)

Figure 3.3 (a) Forward linear *tau-p* transformation. (b) HVF is applied to mute aliasing in linear *tau-p* domain. The horizontal axis is slowness (p) in $\times 10^{-6}$ s/m and the vertical axis is interceptime (τ).

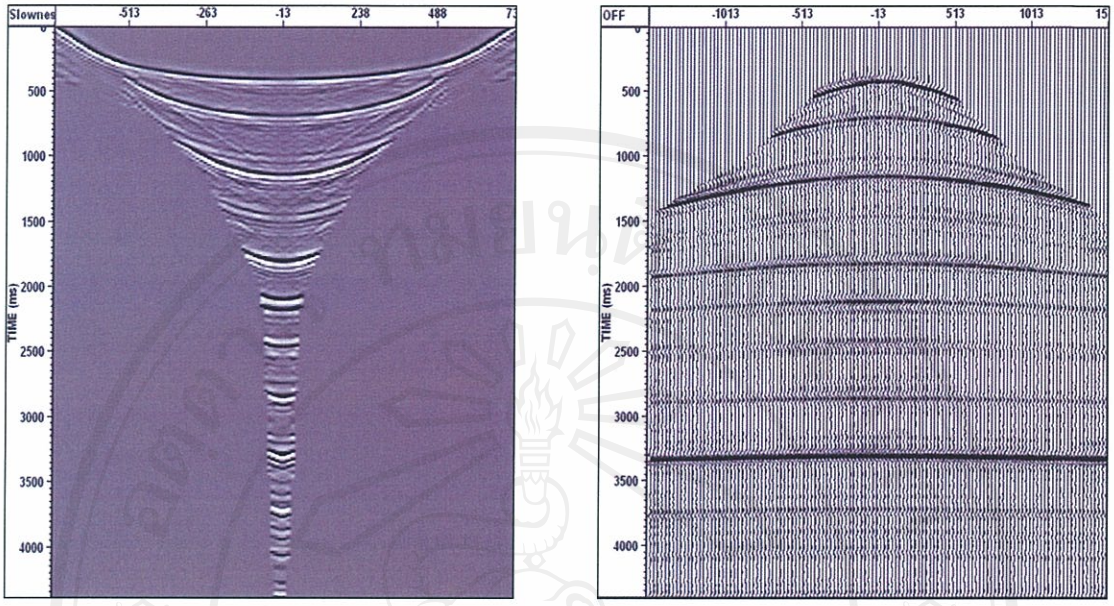

(a) (b)

Figure 3.4 (a) The deconvolution in linear *tau-p* domain where the horizontal axis is slowness (p) in $\times 10^{-6}$ s/m and the vertical axis is interceptime (τ). (b) Inverse linear *tau-p* transformation.

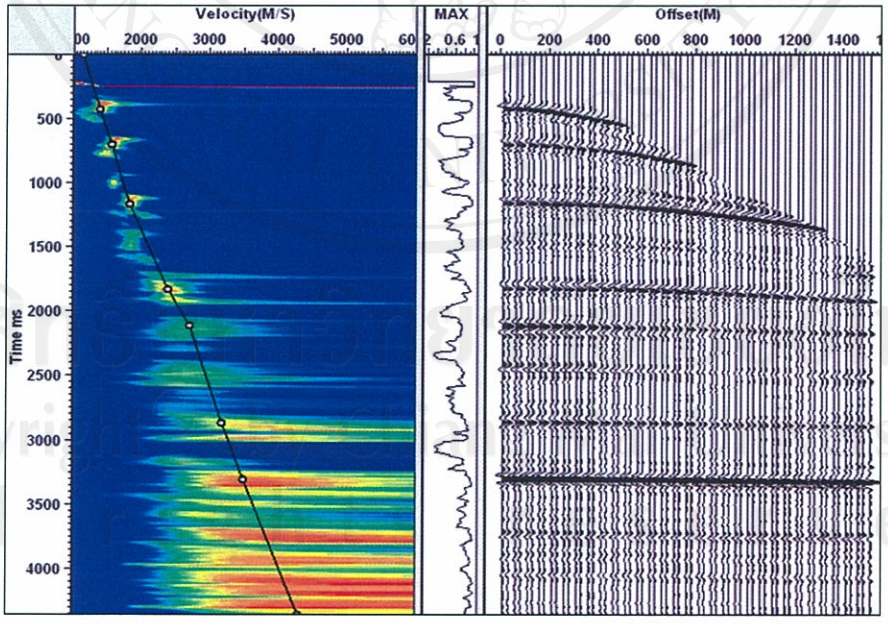

Figure 3.5 Velocity analysis of linear *tau-p* processing in synthetic data, (left) the semblance analysis where the black line is velocity picking and the common offset stacking (right).

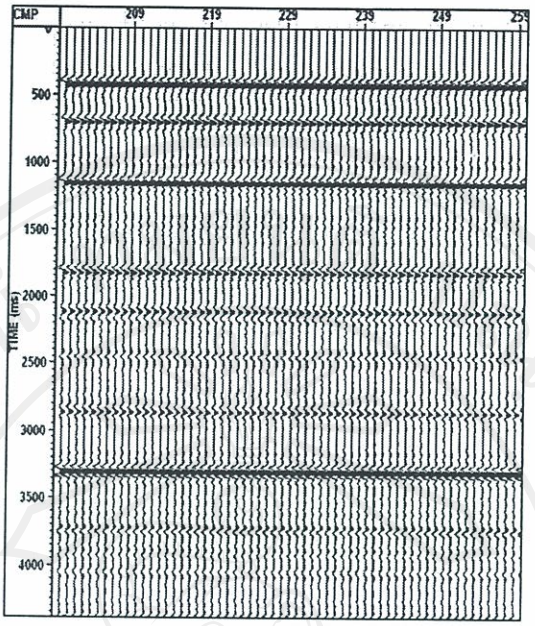

Figure 3.6 Stacking section of synthetic data after linear *tau-p* processing.

3.3 Parabolic *tau-p* processing in synthetic seismic data

The 15 processing steps (Figure 3.1 some processes are not necessary) and the parameters in the parabolic *tau-p* processing are presented in Table 3.2. The sequence for the parabolic *tau-p* processing is described as follows:

Step 1, *Step 2* and *Step3* are similar to linear *tau-p* processing.

Step 4: The NMO correction is applied by using velocity function from velocity analysis in conventional processing (*B.SynVel1* ; Figure 3.7 (a)). The character of reflectors and multiples are separated because the moveout of reflectors are flat and the moveout of multiples are under-corrected (Figure 2.6)

Step 5: Transform seismic data in *t-x* domain to parabolic *tau-p* domain where the character of reflectors is presented at a curvature (q) = 0 s/m^2 and the multiples are presented the curvature more than zero (Figure 3.7 (b)).

Step 6: The frequency aliasing filter are computed from equation (2.39) where the maximum offset (x) is 1500 m, input trace spacing (Δx) is 100 m and the

curvature (q) is 180 ms / 1500^2 m^2, thus will obtain the maximum frequency (f_{max}) is 20 Hz. Therefore the filter bandwidth is 2/7-20/25.

Step 7: Enhancing S/N by sign squaring all data in parabolic *tau-p* domain because relative of the signals energy is increased and random noise is decreased.

Step 8: In the parabolic *tau-p* domain, the character of reflectors and multiples are separated. The multiple muting function is designed by consider the character of multiples in the parabolic *tau-p* domain with the velocity energy spectrum (Figure 3.8). The result from muting is shown in Figure 3.9 (a).

Step 9: Transform from parabolic *tau-p* domain back to *t-x* domain by using same input parameters in *Step 5* and Figure 3.9 (b) shows the result.

Table 3.2 Processing steps and parameters of synthetic data in the parabolic *tau-p* processing.

Processing	Remark
1. Geometry setting and static correction	
2. Trace editing and amplitude recovery	mute refracted wave and exponential gain = 0.5
3. CMP sorting	rearrange data (shot ⟶ CMP)
4. NMO correction	by using velocity function *B.SynVel1*
5. Forward parabolic *tau-p* processing	- reference max offset : 1500 - max, min reference offset : ± 180 ms - moveout increment : 12 ms
6. Filtering	2/7-20/25 (antialiasing Equation 2.39)
7. Sign square	S/N enhanced
8. Multiples muting	
9. Inverse parabolic *tau-p* processing	- reference max offset : 1500 - max, min reference offset : ± 180 ms - moveout increment : 12 ms
10. Sign square root	energy preserved
11. Predictive deconvolution	n = 100 ms, α = 48 ms, ε = 0.1%
12. Filtering	2/7-35/40 Hz
13. Inverse NMO correction	by using velocity function *B.SynVel1*
14. Velocity analysis	output : velocity function *B.SynVel3*
15. Stacking	output : stack section

Step 10: To preserve the relative amplitude variations after parabolic *tau-p* transformation, the sign square root is applied (Figure 3.10 (a)).

Step 11: After inverse parabolic *tau-p* transform, the energy of reflectors is unsharpened and the multiples remained (at nearly $q = 0$ in parabolic *tau-p* domain) then predictive deconvolution is applied.

Step 12: After applying the deconvolution, the bandpass filter is applied.

Step 13: Inverse NMO correction is applied by using the same velocity function in *Step 4* (*B.SynVel1*), the result shown in Figure 3.10 (b).

Step 14: Semblance analysis, common offset stack and common velocity stack compose the velocity analysis to obtain velocity function (*B.SynVel3* ; Figure 3.11).

Step 15: NMO correction by using velocity function *B.SynlVel3* and stacking to obtain the stack section (Figure 3.12).

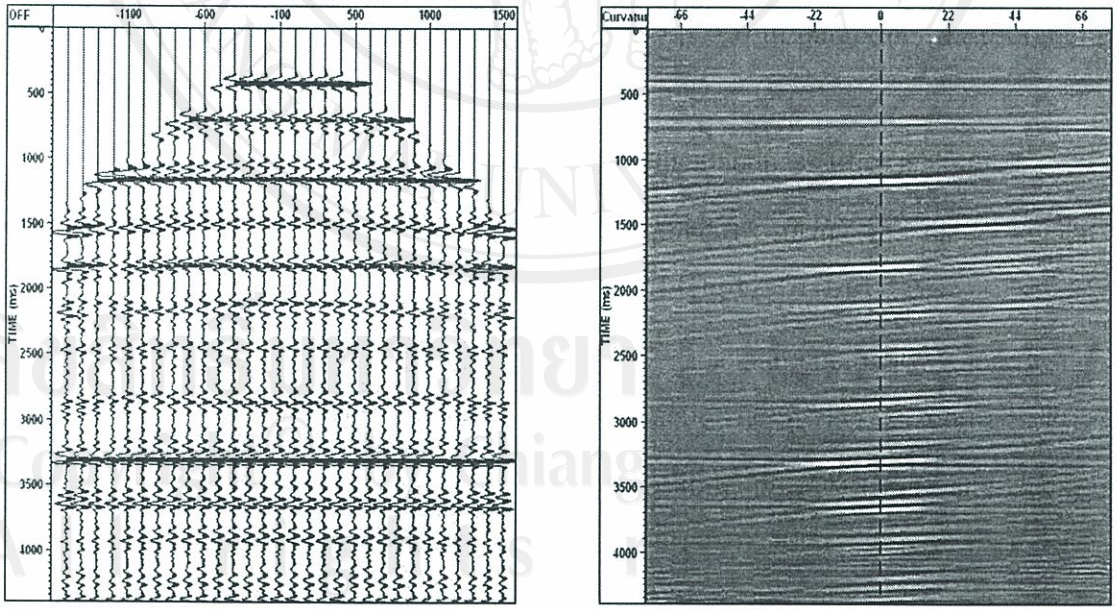

(a) (b)

Figure 3.7 (a) Applying NMO correction in CMP record by using *B.SynVel1*. (b) Forward parabolic *tau-p* transformation where the horizontal axis is curvature (q) in $\times 10^{-9}$ s/m^2 and vertical axis is intercept time (τ).

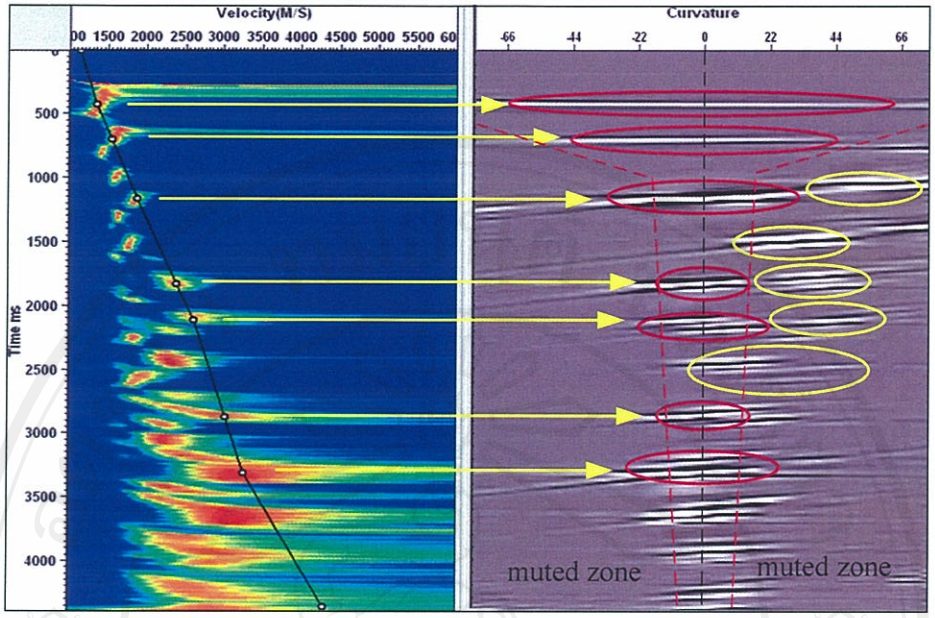

Figure 3.8 Shows the multiples muting (right) are designed with semblance velocity analysis (left). The red dash line is designing muting zone where the red circles are reflectors and the yellow circles are multiples.

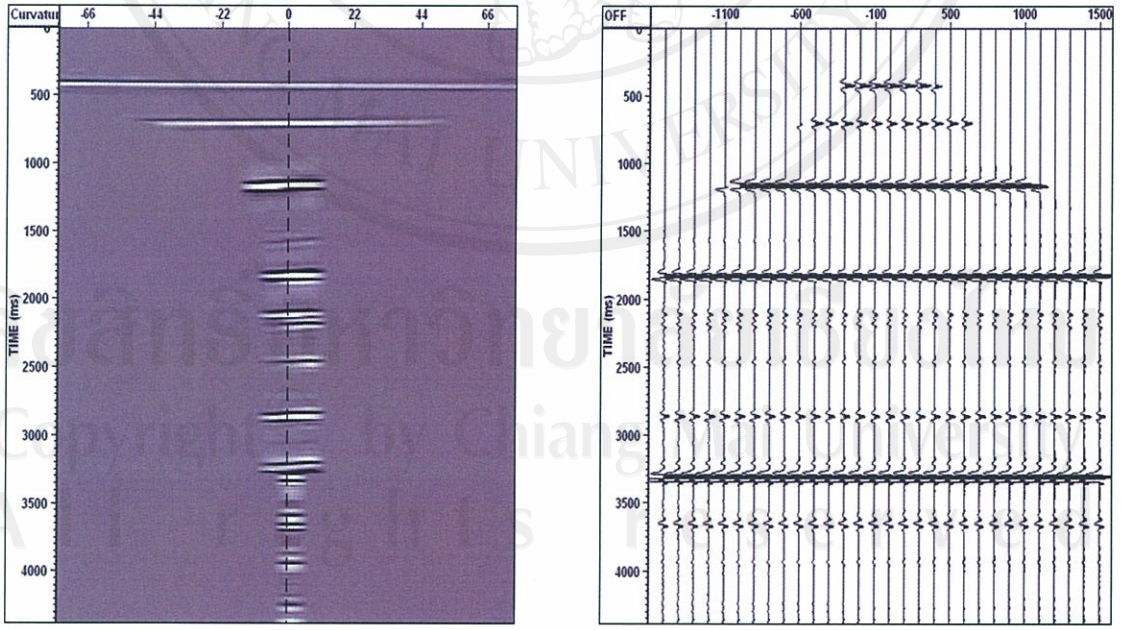

(a) (b)

Figure 3.9 (a) Multiple muting in parabolic *tau-p* domain. (b) Inverse parabolic *tau-p* transform is transformed to *t-x* domain.

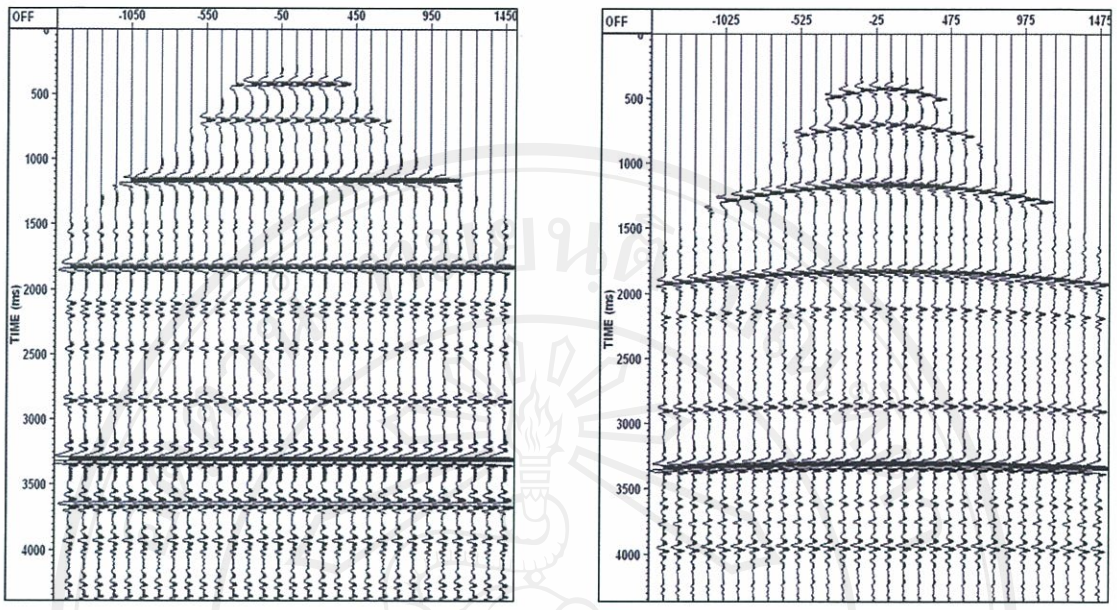

(a) (b)

Figure 3.10 (a) Sign square root is applied to preserve the relative amplitude variations. (b) After applied predictive deconvolution and inverse NMO.

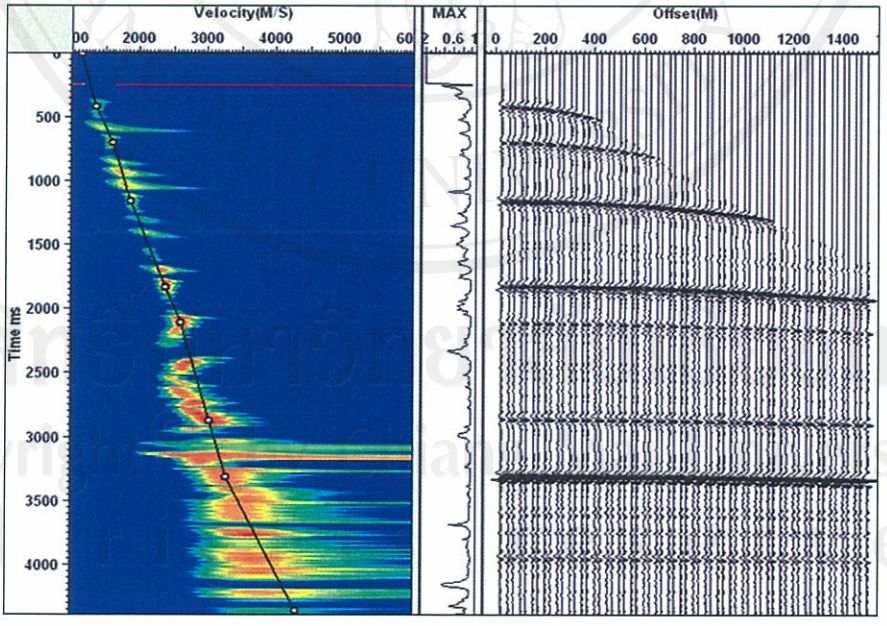

Figure 3.11 Velocity analysis of parabolic *tau-p* processing in synthetic data, (left) the semblance analysis where the black line is velocity picking and the common offset stacking (right).

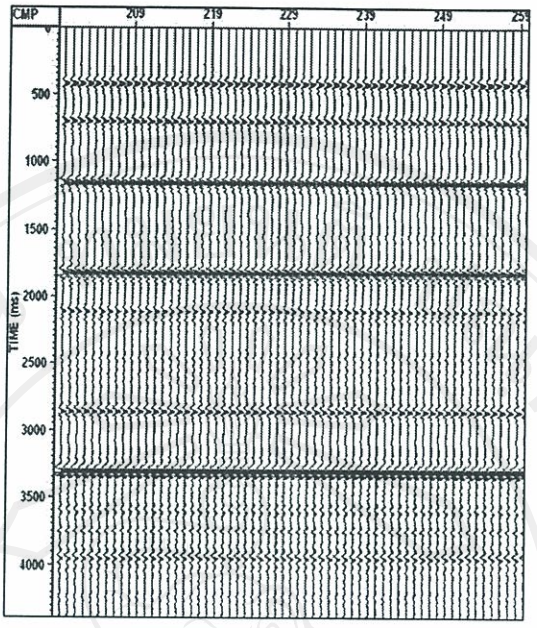

Figure 3.12 Stacking section of synthetic data after parabolic *tau-p* processing.

3.4 Result comparison

The result from the conventional processing, the linear *tau-p* processing and the parabolic *tau-p* processing are compared with non-processing data by presentation in the same parameters display in common shot record (Figure 3.13), velocity energy spectrum (Figure 3.14) and stack section (Figure 3.15).

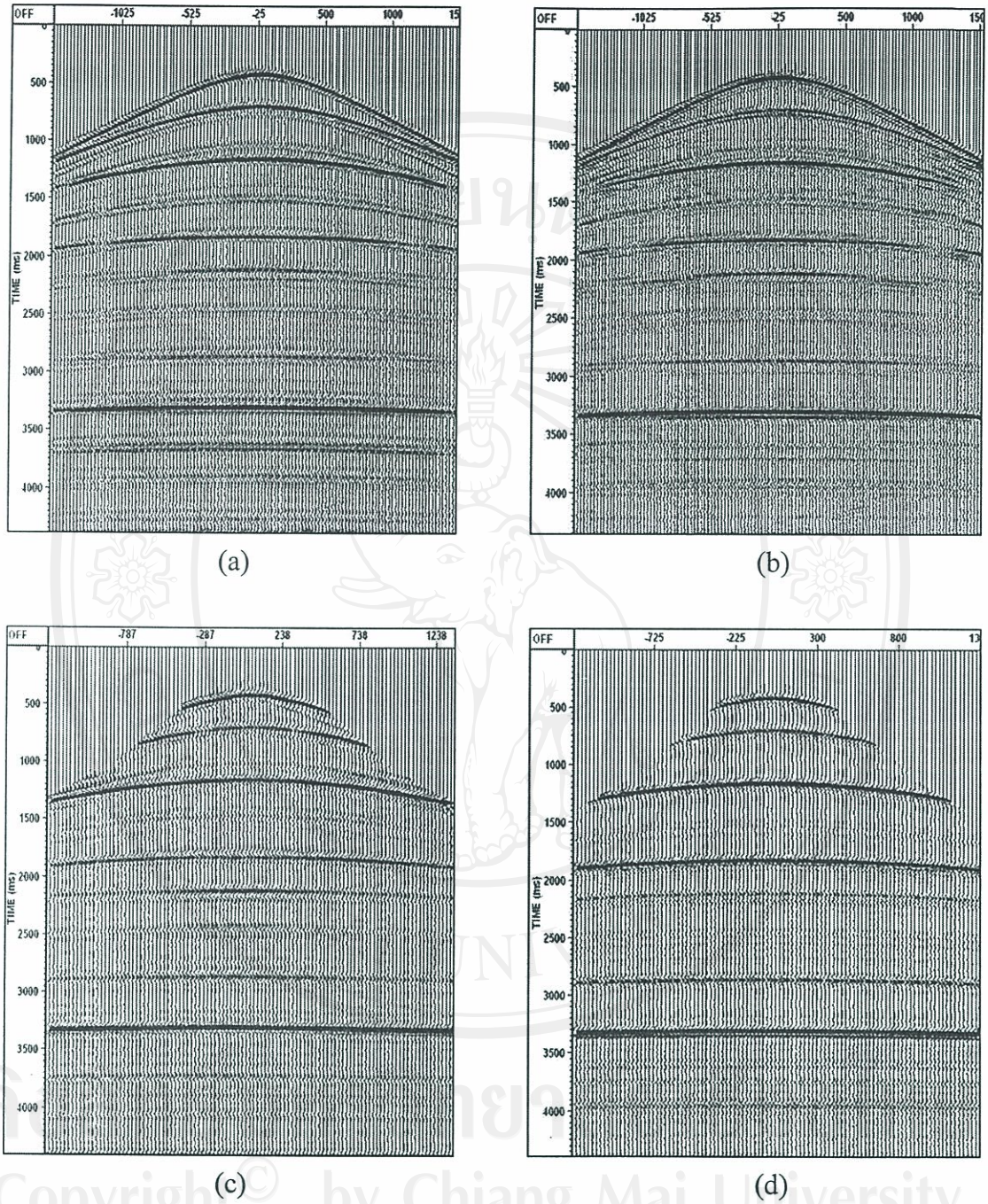

Figure 3.13 Comparing common shot record where (a) non-processing, (b) conventional processing, (c) linear *tau-p* processing and (d) parabolic *tau-p* processing.

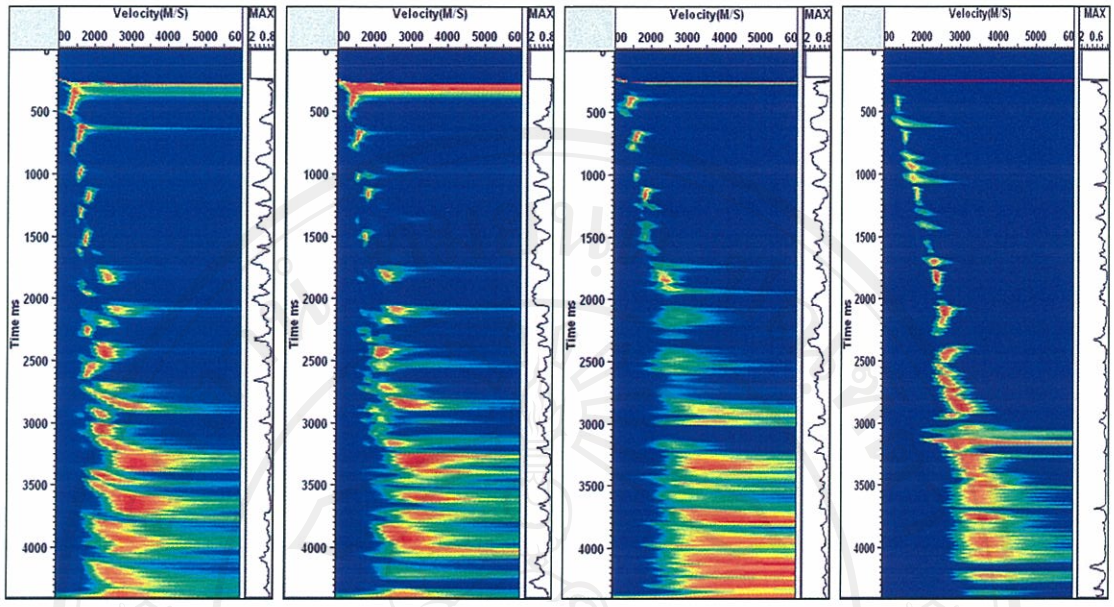

Figure 3.14 Comparing velocity energy spectrum where (a) non-processing, (b) conventional processing, (c) linear *tau-p* processing and (d) parabolic *tau-p* processing.

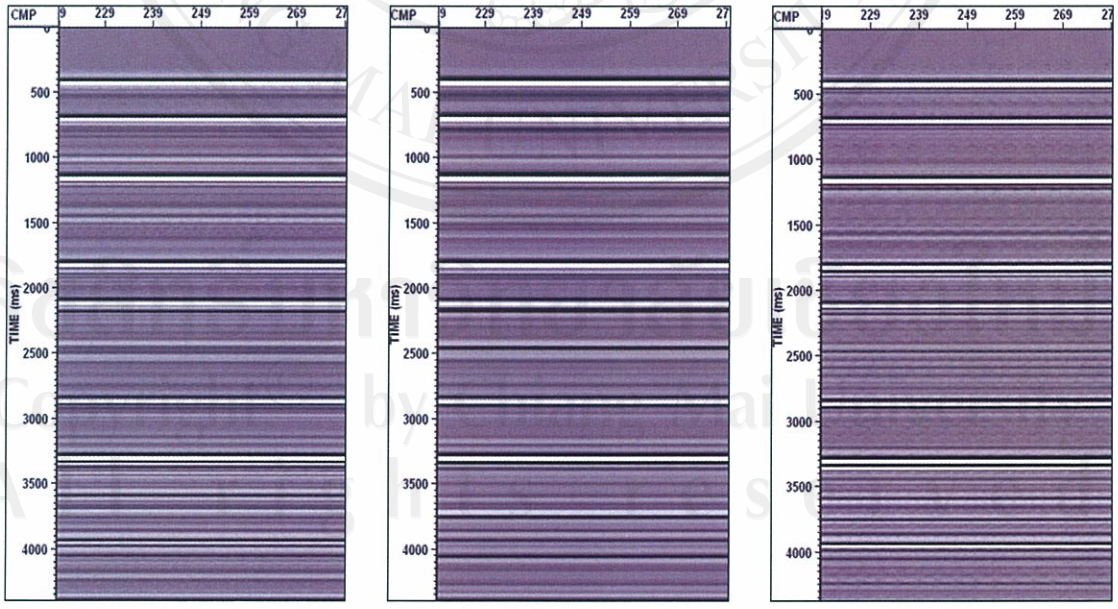

Figure 3.15 Comparing stack section where (a) conventional processing, (b) linear *tau-p* processing and (c) parabolic *tau-p* processing.